P4.26 MULTISPECTRAL THERMAL RETRIEVALS OF SIZE DISTRIBUTION SHAPE, EFFECTIVE SIZE, ICE WATER PATH, OPTICAL DEPTH AND PHOTON TUNNELING CONTRIBUTION

David L. Mitchell[1], Robert P. d'Entremont[2], Daniel H. DeSlover[3], W.Patrick Arnott[1],
1. Desert Research Institute, Reno, Nevada
2. Atmospheric and Environmental Research, Inc., Lexington, Massachusetts
3. Cooperative Institute for Meteorological Satellite Studies, Madison, Wisconsin

1. INTRODUCTION

Satellite and ground-based retrievals from cirrus clouds of effective diameter (D_{eff}) and ice water path (IWP) are needed to describe cirrus radiative properties and to evaluate the role of cirrus in climate. Unfortunately, D_{eff} and IWP are not sufficient for describing ice cloud radiative properties at terrestrial wavelengths. Size distribution shape must also be known for terrestrial radiation (Mitchell 2002), since, for example, the absorption optical depth may differ up to 44% for two cirrus size distributions (SD) having the same D_{eff} and IWP. But even knowing the SD is not sufficient for describing the radiative role of cirrus at terrestrial wavelengths. This is because photon tunneling often contributes 15-42% of the absorption at terrestrial wavelengths (λ), as shown in Fig. 1. Contributions are greatest when particle size and λ are comparable. Photon tunneling accounts for radiation beyond the area cross-section of a particle that is either absorbed or scattered outside of the forward diffraction peak. Baran et al. (2001) have shown that tunneling contributions decrease as ice particle shape becomes more complex. Since ice particle shapes in natural cirrus tend to be complex relative to the pristine shapes assumed in treatments of ice cloud radiative properties based on electrodynamic theory (i.e. at low size parameter), the contribution of the tunneling process to absorption represents a large uncertainty in terrestrial radiation transfer.

In this study we use the modified anomalous diffraction approximation (ADA) for ice clouds (Mitchell 2002), which accurately parameterizes the process of photon tunneling (Mitchell 2000), to quantify the tunneling process in ice clouds by retrieving a tunneling factor, T_f. Modified ADA was validated with laboratory measurements in Mitchell et al. (2001) and with T-matrix theory in Mitchell and Baran (2002). The value of T_f ranges from 1.0 (ice or water spheres) to 0 (no tunneling). Shown below are estimates of tunneling (i.e. T_f) found in natural cirrus clouds.

Corresponding author address: David L. Mitchell, Desert Research Institute, 2215 Raggio Parkway, Reno, NV 89503-1095; e-mail: mitch@dri.edu

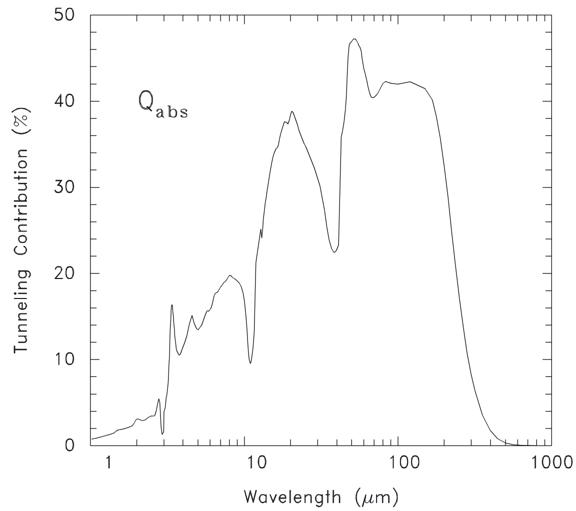

Figure 1. Photon tunneling contribution for a SD of planar polycrystals, large mode mean size = 100 µm.

The proposed methodology provides a means of retrieving D_{eff} and IWP based on the 2nd and 3rd moments (area and mass) of the size distribution, SD. That is, the cirrus emission a sensor receives is from absorption, which ranges from particle area (strong absorption) to mass (weak absorption) dependence. Moderate absorption in the window region (8.3-12.5 µm) would generally exhibit partial area and partial mass dependence. These retrievals are thus sensitive to the small particle mode of the SD ($D < 100$ µm), which retrievals using radar (6th moment dependence) may not be sensitive too. Note that the peak concentration of the small mode is typically 2-3 orders of magnitude greater than the peak concentration in the large SD mode, making D_{eff} based on only the large mode typically about 45% larger than D_{eff} based on both modes, based on measurements of the Forward Scattering Spectrometer Probe (FSSP) and the 2DC probe in mid-latitude cirrus (Ivanova et al. 2001). Hence a radar retrieval of D_{eff} that does not "see" the small mode could seriously overestimate D_{eff}.

Although there is evidence that the FSSP may be accurate in cirrus clouds within a factor of 2-3, a possibility remains that particle shattering at the probe inlet may enhance the numbers of small crystals. In order to test our ideas concerning ice crystal nucleation rates, and to accurately describe ice cloud microphysical and radiative properties, it is critical to determine whether the small SD mode is an artifact due to shattering at the FSSP inlet (or possibly other factors), or whether the high ice particle concentrations measured by the FSSP are real.

The objectives of this study are as follows:

1) Demonstrate the feasibility of retrieving D_{eff}, IWP, visible extinction optical depth τ, and photon tunneling contributions to absorption (T_f) for both ground- and space-based remote sensing.

2) Provide a means of remotely assessing the magnitude and temperature dependence of the small SD mode relative to the large particle mode, to help resolve the role of the small SD mode in determining cirrus microphysical and radiative properties. Do this for both satellite and ground-based remote sensing.

3) Test existing parameterizations of ice particle SDs using thermal radiances from both ground-based and satellite remote sensing.

2. GROUND-BASED RETRIEVALS: AERI

This section describes how the Atmospheric Emitted Radiance Interferometer (AERI; see Smith et al. 1995) can be used to evaluate SD shape, D_{eff}, IWP, T_f and visible extinction optical depth τ. This is shown by way of example, where we have analyzed a mid-latitude cirrus case study (10 Nov. 1995; see DeSlover et al. 1999) and a cold tropical cirrus case study from the CAMEX 3 field program.

Previous studies (e.g. Platt et al. 1989; 1998; 2002; DeSlover et al. 1999; Comstock and Sassen 2001) have used the ratio of visible extinction to thermal absorption optical depth, known as α, to infer ice particle size. However, the ratio of the field of view (FOV) between AERI and the high resolution lidar (HSRL) is 2000 (Edwin Eloranta, private communication), and thus may introduce errors in α (DeSlover et al. 1999). But by using only the retrieved cloud emissivity (and not extinction optical depth), ratios of absorption optical depth, or τ_{abs} ratios, may be obtained spectrally from the AERI (assuming zero scattering). These ratios, often taken at a moderate and a strongly absorbing wavelength, exhibit less scatter relative to the α ratios, and appear to provide reliable estimates of D_{eff}, IWP, T_f and τ

By ratioing τ_{abs} using, for example, the AERI microwindow combinations of 3.9/10.1 μm, or 3.9/11.2 μm, the effective diameter D_{eff} can be retrieved, as shown in Fig. 2. In this work, D_{eff} = (3/2) IWC/(ρ_i P), where ρ_i = density of bulk ice and P = projected area of the size distribution SD. Size information is best retrieved when using a band where absorption is volume or mass dependent, and absorption at 3.9 μm is closest to this condition. In the window region at 10.1 μm, absorption is partially mass and partially area dependent, and is area dependent at 11.2 μm. This causes non-unique solutions for D_{eff} retrievals using the 10.1/11.2 μm ratio, as shown in Fig. 2. Curves were generated using the modified ADA, assuming size distributions parameterized for (1) tropical and (2) mid-latitude (non-convective) cirrus, and assuming 4 ice particle shapes. This provides a measure of expected retrieval uncertainty. As described in Mitchell (2002), SDs having different D_{eff} values can have the same radiative properties (i.e. τ_{abs} ratio) due to the behavior of the small and large particle modes relative to each other.

We have examined the feasibility of using AERI bands around 3.9 μm, and found that radiances emitted by most cirrus are above the clear sky background radiance under nighttime conditions. Also, when AERI bands around 11 μm become saturated (emissivity approaches 1.0), one can switch to the 3.9/10 μm curve for D_{eff} estimates. Sensitivity tests have shown that varying T_f has little

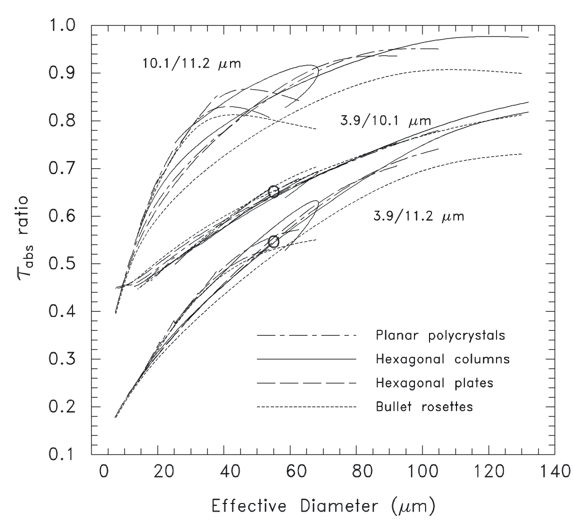

Figure 2. Use of absorption optical depth ratios at various λ for Deff retrievals. Curves are based on two SD parameterizations (tropical and mid-latitude) and four ice crystal shapes to estimate uncertainties. Circles correspond to MODIS retrievals from anvil cirrus using ratios radiatively similar to those indicated.

effect on the 3.9/11 μm curve, while the 3.9/10 μm curve is moderately sensitive (e.g. ±4 μm). The curves in Fig. 2 assume T_f = 0.5.

2.1 *Non-convective Case Study*

Once D_{eff} is retrieved, the tunneling factor T_f can be estimated from AERI spectral τ_{abs} where τ_{abs} is normalized by τ_{abs} at λ = 12.93 μm. This is shown for the window region in Fig. 3. The AERI data (x) are for the 10 November 1995 non-convective cirrus case described in DeSlover et al. (1999), while the solid curve was predicted by modified ADA (Mitchell 2002) for T_f = 0.3, D_{eff} = 65 μm. The short dashed curve predicts normalized τ_{abs} for T_f = 0, while the long-dashed curve is for T_f = 1.0 (maximum value). This illustrates how data between 10.5 and 11.7 μm is sensitive to the value of T_f, and can be used to estimate T_f. AERI data at $\lambda \le$ 10.1 μm is much less sensitive to T_f, but is sensitive to D_{eff}, and can be used to estimate D_{eff}. The 5 data points < 10 μm above the predicted curves are unexplained based on our knowledge of ice refractive indices, and these points were persistently high in the AERI samples. This issue is currently under investigation. Nonetheless, the microwindow at 10.1 μm was consistently in agreement with predicted values, and may be used with greater confidence.

The AERI data from Nov. 10th could be explained using either the mid-latitude SD scheme of Ivanova et al. (2001), or by the tropical SD scheme of Mitchell et al. (2000), using one or more crystal shapes. In this analysis, we used the mid-latitude scheme and assumed hexagonal columns (or compact high density crystals that would have a similar mass- and area-dimensional relationship). Since we were restricted to the window region, dual D_{eff} solutions existed (see Fig. 2). But since the cirrus cloud began thin and steadily deepened, we assume D_{eff} starts off small and grows to larger sizes. Having two D_{eff} solutions has no impact on the retrievals of T_f, since T_f depends on the SD absorption efficiency $\overline{Q}_{abs}$, and a single $\overline{Q}_{abs}$ can correspond to more than one value of D_{eff} (Mitchell 2002).

Knowing D_{eff} and T_f, the modified ADA gives us the area weighted absorption efficiency of the SD, $\overline{Q}_{abs}$ ($\overline{Q}_{abs}$ = absorption coefficient β_{abs}/P), for each AERI microwindow. This information can now be used to determine ice water path (IWP) at each wavelength λ using the formula given in Mitchell and d'Entremont (2000):

$$\mathrm{IWP} = \frac{2\,\rho_i\,D_{eff}\ln(1-\epsilon)\cos\theta}{3\,\overline{Q}_{abs}} \qquad (1)$$

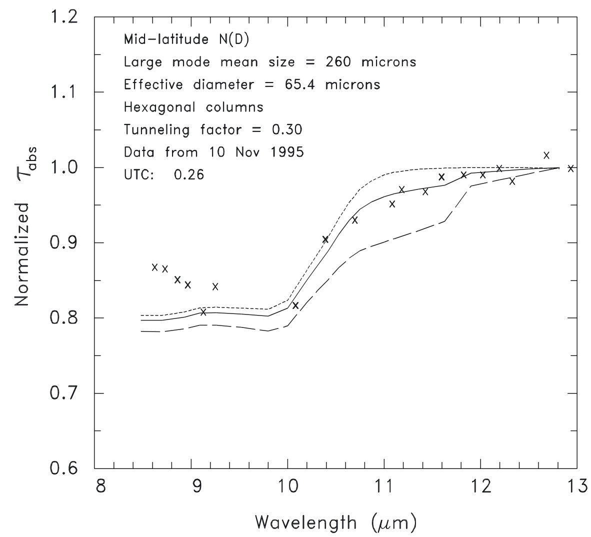

Figure 3. Retrieval of tunneling factor from an AERI sample, with τ_{abs} normalized to the longest λ. Dashed curves indicate range of tunneling contributions.

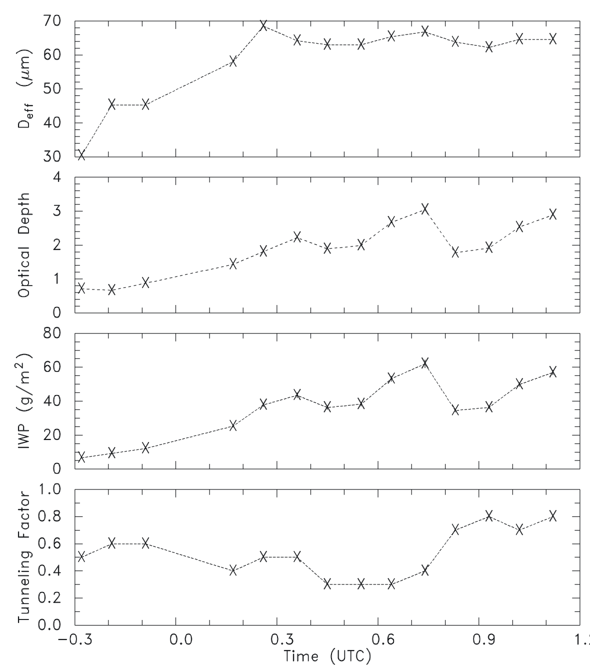

Figure 4. Evolution of non-convective cirrus case based on multispectral AERI retrievals.

where ϵ = cloud emissivity and θ = instrument viewing angle (θ = 1 at zenith). IWPs at each λ can be averaged (if $\epsilon(\lambda)$ is unsaturated) to produce a mean IWP, and an estimate of precision is obtained from the standard deviation. For this case study, the precision was about ±5%. For optically thick cirrus,

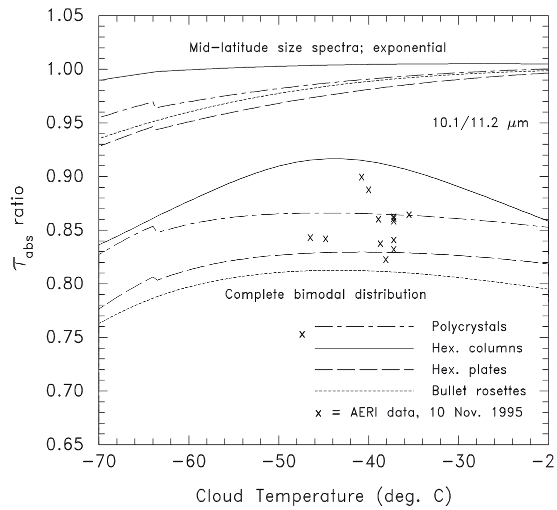

Figure 5. Comparison of τ_{abs} ratios predicted for SI with and without the small mode as measured by tl FSSP. Measured τ_{abs} ratios are given by the symbols.

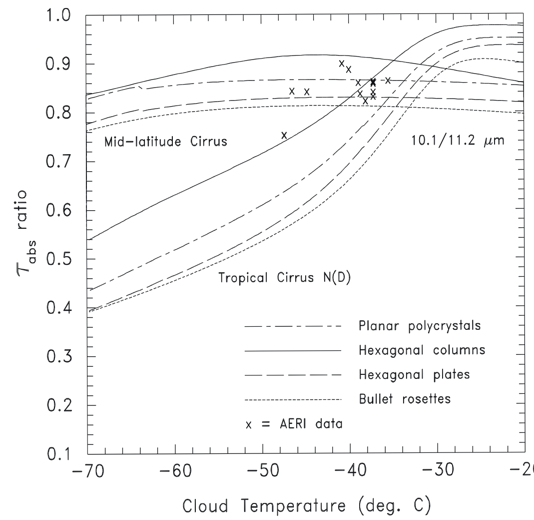

Figure 6. Temperature dependence of τ_{abs} ratio (10.1/11.2 μm) as predicted by SD schemes for tropical and mid-latitude cirrus. Ratios from the mid-latitude AERI case study of 10 November are plotted (x).

$\lambda \approx 3.9$ μm can be used to obtain ϵ and $\overline{Q}_{abs}$, so that IWP values at least up to 100 g m^{-2} can be retrieved.

Finally, visible optical depth τ is estimated from the retrieved IWP and D_{eff}:

$$\tau = 3\ \mathrm{IWP}/(\rho_i\ D_{eff}) \qquad (2)$$

which is based on the assumption that at visible wavelengths, extinction efficiency $Q_{ext} = 2$.

The results of our analysis of the 10 November cirrus case are described in Fig. 4. This methodology is the first to estimate the contribution of photon tunneling to natural ice clouds, quantified using T_f. Since T_f depends on the complexity of ice particle shape (Baran et al. 2001), the variation of T_f in Fig. 4 may reflect variations in crystal shape. The mean value of T_f in Fig. 4 is 0.53 ±0.18. In Mitchell et al. (2001), T_f was found to be about 0.6 for hexagonal columns grown in a cloud chamber. However, a T_f of 0.8 fit the extinction efficiencies in the window region the best.

2.1.1 Size distribution shape

A major question relevant to the disciplines of cloud physics, atmospheric radiation, and climate prediction is whether the high ice particle concentrations N measured by the FSSP probe are real. If the answer is yes, then ice particles having maximum dimension D < 100 μm account for a large percentage of the SD projected area P, and thus will have a major impact on cirrus cloud radiative properties. Fortunately, this question can be addressed through AERI measurements, which provide information of SD shape. The mid-latitude SD scheme of Ivanova et al. used FSSP measurements to characterize the small mode, and the 2DC probe to characterize the large SD mode. If small mode N is orders of magnitude greater than large mode N, then the SD area weighted absorption efficiency, $\overline{Q}_{abs}$, will be considerably less than 1.0 in the window region for λ between 8.3 and 10.2 μm, while $\overline{Q}_{abs}$ for $\lambda \approx 11$ μm will be generally be near 1.0. For example, the 10.1/11.2 μm τ_{abs} ratio obtained via AERI will be $\lesssim 0.93$ if small mode N is high. Such AERI data from the 10 November case study is plotted in Fig. 5, along with corresponding τ_{abs} ratio curves from modified ADA and the mid-latitude SD scheme for various ice particle shapes. The SD temperature dependence in Ivanova et al. allows us to plot the τ_{abs} ratio against temperature. A sounding released during the AERI case study (Madison Wisconsin) was used to estimate the temperature corresponding to the clouds "radiative center of mass", as estimated from lidar backscatter (DeSlover et al. 1999). Also plotted are curves (in upper figure) that are based on exponential size spectra. These spectra are calculated from the mean particle size $\overline{D}_l$ measured by the 2DC probe and the associated SD slope (SD slope = $1/\overline{D}_l$), which was parameterized in terms of temperature in Ivanova et al. (2001). These exponential SDs insure that N increases with decreasing size, but by definition are not bimodal, so that small mode N is not orders of magnitude higher than large mode N.

The difference between the exponential and bimodal SD curves in Fig. 5 demonstrate the impact of the small mode on the τ_{abs} ratio. It is seen that using the small mode based on the FSSP renders good agreement with the measured τ_{abs} ratios (x symbols) for non-convective cirrus. The vertical scatter in the measured ratios could be due to changes in ice crystal shape, or due to changes in small mode $\overline{D}$ and N. The point for the coldest temperature (lowest τ_{abs} ratio) was obtained when the cloud was thinnest near the beginning of its life cycle.

Finally, the τ_{abs} ratio 10.1/11.2 μm is predicted to behave differently as a function of temperature for tropical convective (Mitchell et al. 2000) vs. non-covective mid-latitude cirrus (Ivanova et al. 2001), based on modified ADA. This is shown in Fig. 6. The temperature dependence of this measured τ_{abs} ratio (x symbols in Fig. 6) reveals the temperature dependence of the small SD mode relative to the large SD mode, and whether this behavior conforms to that predicted for the tropical or mid-latitude cirrus schemes. It is seen that the AERI data conform well with the predicted mid-latitude curves. One reason for the different temperature dependencies in Fig. 6 is that the small particle mode in the mid-latitude SD scheme becomes more pronounced (higher concentrations) as the large SD mode broadens (SD slope decreases). The opposite is true for the tropical SD scheme, where the small mode diminishes as the large mode broadens. These differing behaviors result in a much different temperature dependence regarding D_{eff} and SD shape, with D_{eff} in the mid-latitude scheme varying much less with temperature than D_{eff} for the tropical SD scheme. Both D_{eff} and SD shape contribute to the differences between SD schemes in Fig. 6.

Even if the retrieved τ_{abs} ratios did not correspond to either SD scheme, it is possible to modify the tropical or mid-latitude SD parameterization, based on the retrieved D_{eff} and τ_{abs} ratios, and the large mode mean length $\overline{D}_l$ given by the parameterization as a function of temperature. Note that $\overline{D}_l$ is based on measurements from the 2DC probe, which are fairly reliable. First, it is helpful to note that the τ_{abs} ratio is the same as the corresponding $\overline{Q}_{abs}$ ratio. For two SDs having the same D_{eff}, $\overline{Q}_{abs}$ will be lower in the SD having higher ice crystal concentrations N (i.e. steeper slope) in the small particle mode (Mitchell 2002). Thus $\overline{Q}_{abs}$ is both a function of D_{eff} and SD shape. By retrieving both D_{eff} and the τ_{abs} ratio, the SD shape can be inferred by manipulating the relative contribution of small mode N in our radiation scheme to yield curves conforming with the observed temperature dependence of the τ_{abs} ratios and D_{eff} values. To estimate temperatures corresponding to retrieved τ_{abs} ratios and D_{eff}, a sounding and vertical lidar (or radar) backscatter profile are needed to estimate the temperature of the cloud's radiative center of mass. With this information, one can modify the existing SD schemes such that they fit the AERI retrievals.

2.2 *Convective Case Study*

During the CAMEX 3 field experiment, cirrus outflow from Hurricane Bonnie was sampled by the AERI on 23 August 1998 near the Bahama Islands, and soundings were taken during the sampling period. The cirrus were several km thick, centered around 14 km altitude with mid-point temperatures around -60 ^{o}C. Due to the cold temperatures, cirrus emittance was lower than for the mid-latitude case centered around -40 ^{o}C, making the AERI signal noisy relative to the mid-latitude case. But optical depth was more than 1.0, and some periods of sampling contained useful data. For this case, the microwindow at 9.1 μm appeared more stable than the microwindow at 10.1 μm, and D_{eff} retrievals were based on the 9.1/11.2 μm τ_{abs} ratio. The curves relating D_{eff} to the τ_{abs} ratio were for tropical cirrus, similar to the 10.1/11.2 μm τ_{abs} ratio curves in Fig. 2 for tropical cirrus (i.e. the curves extending to the largest D_{eff} values). D_{eff} estimates were unique with uncertainties ± 13% for D_{eff} < 60 μm (due to particle shape). Planar polycrystals were assumed.

D_{eff} was also estimated using all window region wavelengths, as illustrated in Fig. 7. The 3 curves correspond to a T_f of 0 (short-dashed), 0.5 (solid) and 1.0 (long-dashed). Both D_{eff} and T_f were optimized to produce the best match between theory and observations. Fig. 7 is typical of this case in that τ_{abs} ratios (normalized by τ_{abs} at λ = 12.93 μm) appeared anonymously high relative to theory for wavelengths between 8.6 and 10.1 μm. We note that the τ_{abs} ratio at λ = 9.1 μm was consistently the lowest, and this point was considered valid when matching theory with observations. It is not clear why other τ_{abs} ratios for λ < 10.3 μm appear anonymously high, but the high contribution of background emission and potential ozone emission may be factors.

The analysis illustrated by Fig. 7 was also used to estimate T_f. When estimating T_f, we used the "least noisy" AERI data, which corresponded to wavelengths at 9.1 μm and 10.3 μm < λ < 11.9 μm. Still, the uncertainty in estimating T_f was greater here than in the mid-latitude case. The T_f estimated for

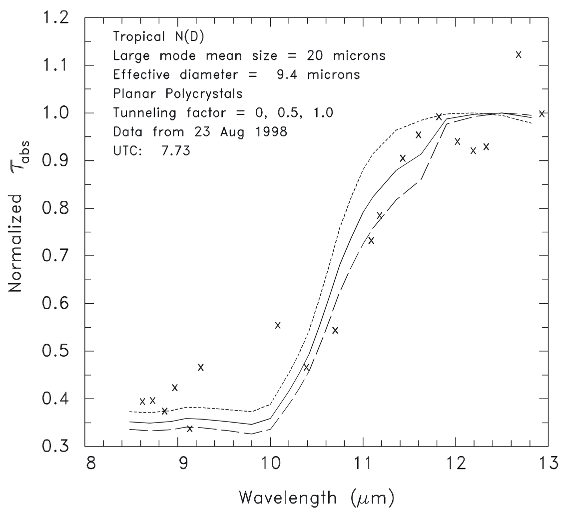

Figure 7. Retrieval of T_f from a tropical cirrus AERI sample, with τ_{abs} normalized to the longest λ. Dashed curves indicate range of tunneling contributions; solid curve gives T_f = 0.5. For this sample, T_f was estimated as 0.7.

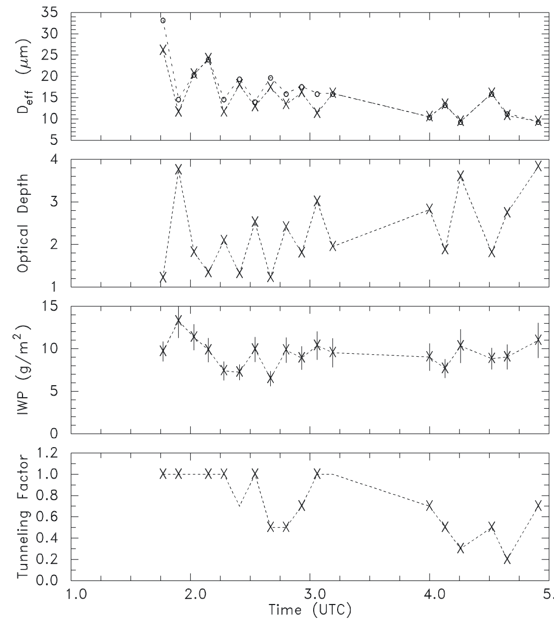

Figure 8. Evolution of cirrus outflow from Hurricane Bonnie, based on AERI retrievals.

the AERI sample in Fig. 7 was 0.7.

Retrieval results for this tropical cirrus case study are shown in Fig. 8. The 0.8 hour sampling gap between 3.2 and 4.0 hours UTC was actually 3.6 hours, but is shown here as 0.8 h to present the results more clearly. As noted, D_{eff} was determined two ways: using only two wavelengthts, and using all λ as illustrated in Fig. 7. The circle symbols correspond to the two λ approach, while the X symbols correspond to the all λ approach. It is seen that the two λ approach, relevant to satellite retrievals, is sufficient for most applications. As noted, IWP was calculated for all 19 λ. Mean values and their standard deviations are shown in the IWP panal. Given the challenging operating conditions for the AERI, the IWP uncertainties are quite low. Tunneling factors for this case varied considerably, and were generally larger than in the mid-latitude case (mean T_f = 0.74 ± 0.27).

There is some evidence of periodicity in the results for D_{eff}, τ and possibly IWP. This might be explained by gravity waves emanating from Hurricane Bonnie, although this is only a guess at this time. If we interpret the data this way, with decreases in D_{eff} corresponding to increases in IWP, there is an implication that ice crystal nucleation rates increase with increasing condensation rates, driving down the mean ice particle size.

2.2.1 Size distribution shape

As noted, the tropical cirrus SD scheme described in Mitchell et al. (2000) predicts that the small and large particle modes in anvil cirrus behave in the opposite manner relative to non-convective mid-latitude cirrus as described in Ivanova et al. (2001). That is, as the large mode (D > 100 μm) broadens with increasing temperature T in anvil cirrus, the number concentration N in the small SD mode diminishes. This may be due to size-sorting by fall speed, with the larger particles descending faster and accumulating preferentially in the mid-to-lower cloud, while the smallest crystals tend to remain aloft at the main detrainment level. Also, aggregation by larger ice particles is likely to deplete the smaller crystals. This physical reasoning supports the above observation in anvil cirrus. In mid-latitude cirrus, the opposite occurs, with small mode N increasing as the large mode broadens (slope decreases) with increasing T. To understand the microphysics and radiative properties of convective and non-convective cirrus, we need to know whether these differences are real or simply artifacts of the FSSP.

Figure 9 shows the τ_{abs} ratio 9.1/11.2 μm predicted by modified ADA for mid-latitude and tropical cirrus for 4 different ice crystal shapes, giving an estimate of expected uncertainty. Also shown are the AERI τ_{abs} ratios corresponding to 9.1/11.2 μm (x symbols). These are plotted at the mid-cloud temperature, which is based on soundings launched during sampling and lidar backscattering returns. The AERI data clearly support the tropical anvil SD scheme, and the implied physics described above. The tropical SD scheme predicts very high

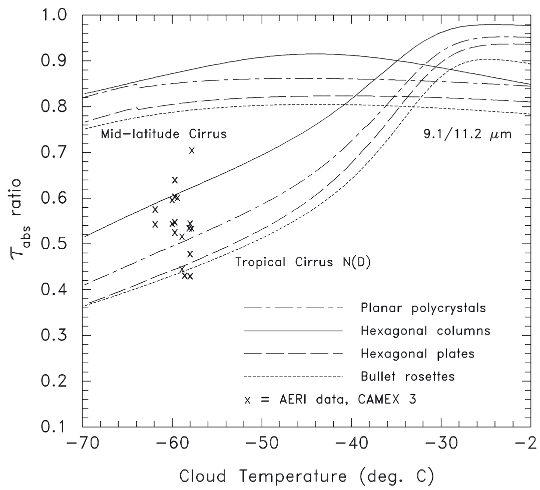

Figure 9. Comparison of AERI τ_{abs} ratios (x) from Hurricane Bonnie outflow with ratios predicted from the mid-latitude and tropical cirrus schemes.

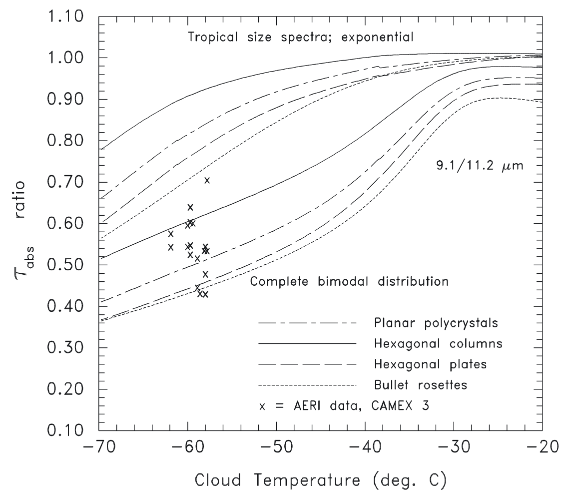

Figure 10. Comparison of τ_{abs} ratios predicted for the tropical SD scheme, with and without the small SD mode. Measured ratios from Hurricane Bonnie outflow are given by the x symbols.

N in the small mode at these temperatures, with the small mode dominating the SD area. The scatter in the AERI data may be due to variations in particle shape or small mode N.

Figure 10 is similar to Fig. 9 except the τ_{abs} ratio is predicted for the tropical scheme with only the large particle mode, which an exponential function. The absence of the small mode is seen to raise the τ_{abs} ratio considerably. The AERI data support the parameterization of the small mode and the tropical SD scheme in general. Moreover, the AERI data indicate the presence of very high concentrations of small crystals in tropical cirrus, that are generally too small to be detected by the 2DC probe.

3. SATELLITE RETRIEVALS: MODIS

Similar methodology to that above can be used with MODIS satellite data to retrieve D_{eff}, T_f, IWP and SD shape information. This methodology will be demonstrated using a MODIS satellite scene from the western north Atlantic featuring cirrus of convective origin (associated with the Gulf Stream) during 13 October 2000. Using a methodology similar to d'Entremont et al. (1990), τ_{abs} can be obtained for each MODIS channel. This method solves the equation

$$I_{obs} = (1-\epsilon)I_{sfc} + \epsilon B_{ci} \qquad (3)$$

at two wavelengths, where ϵ is bulk cirrus emissivity, I_{obs} is the upwelling thermal radiance from cloud, I_{sfc} is the upwelling radiance emitted by the underlying surface (i.e. either the ground or a low level cloud) and clear atmosphere, and B_{ci} denotes the cirrus Planck blackbody radiance, which is a known function of the cirrus effective temperature T_{ci}. The two measured quantities in (2) are I_{obs} and I_{sfc}, corresponding to cloudy or adjacent cloud-free scenes, respectively. This results in two equations (one for each λ) and two unknowns (ϵ and B_{ci}). Unique solutions for ϵ and B_{ci} are achieved due to (1) the Planck function dependence on temperature at widely separated wavelengths, and (2) the dependence of ϵ on wavelength. The ϵ (common to both λ) corresponding to T_{ci} is then used in a radiation transfer model incorporating radiances from other MODIS channels, with ϵ in each channel forced to be consistent with all observed radiances, the initial ϵ retrieval, and radiation transfer theory using modified ADA. From the resulting ϵ retrievals, τ_{abs} is obtained assuming zero scattering, provided ϵ is significantly < 1.0. While τ_{abs} retrievals are not sensitive to ice particle shape assumptions, there is a weak sensitivity to SD shape (i.e. convective vs. stratiform cirrus), which is diagnosed from retrieved properties like cloud temperature and altitude, and the general appearance of the cloud field in the satellite scene.

The D_{eff} retrievals illustrated in Fig. 2 can also be applied to satellite retrievals. For instance, the MODIS instrument has channels at 3.74, 8.55, 11.0 and 12.0 µm, allowing τ_{abs} ratios similar to those used in Fig. 2 to be formed (note refractive indices at 10.1 and 8.5 µm are very similar). As described above, τ_{abs} was retrieved for these MODIS channels. An arbitrary sample of about 800 pixels gave mean τ_{abs} ratios of 3.7/8.5 µm and 3.7/11 µm of 0.655 and

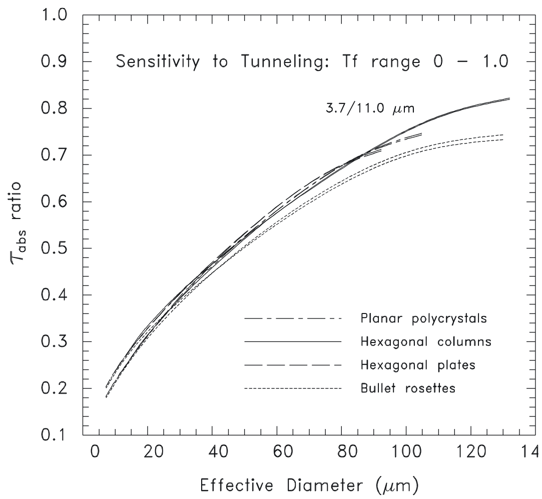

Figure 11. Curves for MODIS D_{eff} retrievals based on tropical SD scheme. Each crystal type has 2 curves: with maximum tunneling and with no tunneling.

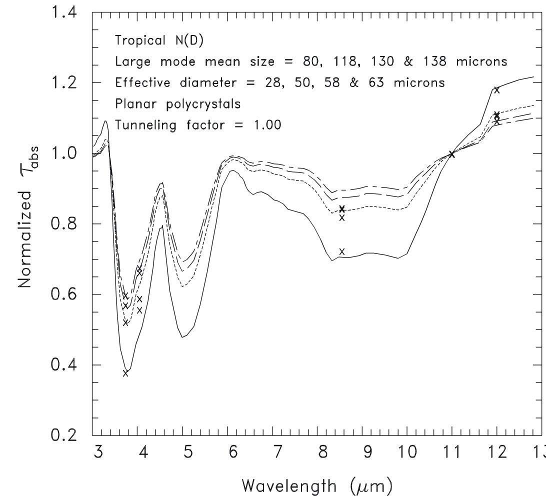

Figure 12. Predicted curves of $\tau_{abs}(\lambda)$, normalized to τ_{abs} at 11.0 μm, for the retrieved D_{eff} listed (lower curves for smaller D_{eff}), using T_f = 1.0. MODIS observations (x) are sensitive to T_f at 12 μm.

0.550, respectively. These are indicated by the "o" symbols in Fig. 2. The fact that these ratios both correspond to D_{eff} = 55 μm is encouraging.

As a proof of concept exercise, we evaluated this anvil cirrus MODIS image, stratifying the emissivity retrievals for each channel into 4 bins based on the 11 μm emissivity: 0-0.2, 0.2-0.5, 0.5-0.8, and 0.8-1.0. A D_{eff} was retrieved for each bin using the predicted τ_{abs} 3.74/11.0 μm ratio for anvil cirrus, shown in Fig. 11 (essentially the same as the 3.9/11.2 μm curves in Fig. 2). Each crystal type in Fig. 11 has two curves: one assuming zero tunneling and one assuming maximum tunneling (T_f = 1.0). It is seen that tunneling has little effect on D_{eff} retrievals, except at the smallest sizes. This is because tunneling is minimal at both wavelengths; due to the large size parameter at 3.7 μm, and due to the low real refractive index at 11 μm.

Next, MODIS τ_{abs} at 3.74, 4.05, 8.55, 11.0 and 12.0 μm were normalized to τ_{abs} at 11 μm to determine T_f and to confirm the D_{eff} retrievals. This data is plotted in Fig. 12 for each emissivity bin. The retrieved D_{eff} values are listed, and predicted τ_{abs} curves are shown for each D_{eff} retrieval. The lowest curve corresponds to the smallest D_{eff} value, the highest curve to the largest D_{eff}. Since the tunneling process depends on D_{eff}, the use of four retrieved D_{eff} values to generate four τ_{abs} curves provides a more rigorous estimate of T_f.

The difference in τ_{abs} between 11 and 12 μm is a measure of the tunneling contribution and T_f. This is because without tunneling, $\overline{Q}_{abs}$ would be about 1.0 at both wavelengths in most cirrus. The difference in brightness temperature and τ_{abs} at these wavelengths is almost entirely due to differences in tunneling contributions (see Fig. 1). In this 2nd step of the MODIS retrieval, T_f is varied between 0 and 1 in order to find the T_f that best describes the MODIS data.

With these steps complete, modified ADA is then used to determine the SD $\overline{Q}_{abs}$ for each of the above MODIS bands. The retrieved D_{eff}, and corresponding emissivities, are then used with $\overline{Q}_{abs}$ in Eq. (1) to calculate IWP for each channel, and a mean IWP is determined.

Retrievals of T_f are shown in Fig. 12. Matching between theory and observations at λ = 12 μm depends strongly on T_f, with a T_f of 0.8 producing a clear mismatch (not shown). A T_f of 1.0 fits the MODIS data best, as shown in Fig. 12. This was unexpected, as laboratory measurements and electrodynamic theory both indicate T_f should be less than 1.0 for hexagonal columns and plates (Mitchell et al. 2001; Baran et al. 2001). One possible explanation is that convective cirrus, formed through the detrainment of condensed water from the convective updraft column, may be comprised of high concentrations of frozen droplets or quasi-spherical particles that dominate the SD area. While larger crystal shapes are non-spherical, concentrations of quasi-spherical particles with D < 50 μm may be high enough to dominate the anvil infrared radiative properties as seen from space. Clearly more satellite scenes and analysis are needed to understand this issue.

Finally, the SD shape can be inferred using MODIS channels, such as those at 3.74 and 11.0 μm, using the methodology described under AERI retrievals and retrievals of T_{ci}. This is illustrated in Fig. 14. While more points are needed, the present MODIS data are consistent with the SD scheme for tropical (i.e. anvil) cirrus. This is encouraging, since most of the cirrus in the satellite scene were of convective origin. The low τ_{abs} ratios relative to mid-latitude values indicate higher concentrations of smaller crystals in the small mode for anvil cirrus. The points near -50 and -40 ^{o}C correspond to the ϵ bins 0-0.2 and 0.8-1.0, respectively. The number of pixels used in each ϵ bin, from lowest to highest ϵ, are 1148, 8100, 8861, and 17474, respectively.

4. SUMMARY

A relatively accurate method of retrieving IWP has been described and implemented for ground-based and satellite remote sening, with uncertainties (standard deviation) < ± 20%, applicable over an IWP range of at least 1-100 g m^{-3} when using a channel around 3.9 µm. Effective size and optical depth are also retrieved in this process.

Methods were introduced allowing two new cloud properties to be retrieved for the first time: (1) size distribution shape or bimodality, and (2) photon tunneling contribution to absorption, quantified as a tunneling factor T_f. Results regarding (1) suggest that the high concentrations of small crystals (D < 60 µm) measured by the FSSP are real (not primarily artifacts of ice particle shattering at the probe inlet), and that their radiative impact is important. These results also support existing parameterizations of cirrus size spectra of convective and non-convective origin, providing evidence that the physical processes governing the evolution of size spectra in these two cirrus categories are fundamentally different. Future retrievals regarding (2) may reduce much of the uncertainty that plagues radiation transfer in ice clouds at thermal wavelengths.

AKNOWLEDGMENT

This work was funded by the Department of Energy, Atmospheric Radiation and Measurement (ARM) Program, which is gratefully thanked for their support.

REFERENCES

Baran, A.J., S. Havemann, P.N. Francis, and P. Yang, 2001: A study of the absorption and extinction properties of hexagonal ice columns and plates in random and preferred orientation, using exact T-matrix theory and aircraft observations of cirrus. *JQSRT*, **70**, 505-518.

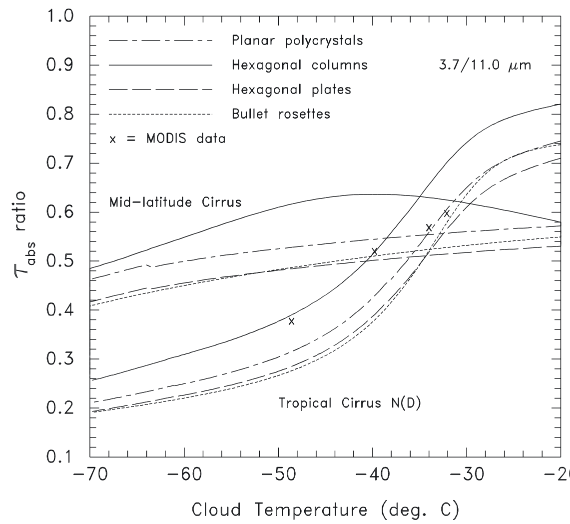

Figure 13. Temperature dependence of the τ_{abs} ratio as predicted by the SD schemes for tropical and mid-latitude cirrus. Corresponding MODIS data are compared.

Comstock, J.M., and K. Sassen, 2001: Retrieval of cirrus cloud radiative and backscattering properties using combined lidar and infrared radiometer (LIRAD) measurements. *J. Atmos. Ocean. Tech.*, **18**, 1658-1673.

D'Entremont, R.P., M. Griffin, and J.T. Bunting, 1990: Retrieval of cirrus radiative properties and altitudes using multichannel infrared data. Preprints, 5th Conf. Sat. Meteor. And Ocean., 3-7 Sept., London, Amer. Meteor. Soc.

DeSlover, D., W.L. Smith, P.K. Ppiironen and E.W> Eloranta, 1999: A methodology for measuring cirrus cloud visible-to-infrared spectral optical depth ratios. *J. Atmos. Ocean. Tech.*, **16**, 251-262.

Ivanova, D., D.L. Mitchell, W.P. Arnott and M. Poellot, 2001: A GCM parameterization for bimodal size spectra and ice mass removal rates in mid-latitude cirrus clouds. *Atmos. Res.*, **59**, 89-113.

Mitchell, D.L., 2000: Parameterization of the Mie extinction and absorption coefficients for water clouds. *J. Atmos. Sci.*, **57**, 1311-1326.

Mitchell, D.L., D. Ivanova, A. Macke and G.M. McFarquhar, 2000: A GCM parameterization of bimodal size spectra for ice clouds. Proceedings of the 9th ARM Science Team Meeting, March 22-26, 1999, San Antonio Texas (http://www.arm.gov/docs/documents/technical/conference.html).

Mitchell, D.L., and R.P. d'Entremont, 2000: Nighttime retrieval of ice water path. Proceedings, *5th Conference on Electromagnetic and Light Scattering by Nonspherical Particles: Theory, Measurements and Applications*, AMS, August 28 - September 1, 2000, Halifax, Nova Scotia, Canada, 168-172.

Mitchell, D.L., W.P. Arnott, C. Schmitt, A.J. Baran, S. Havemann and Q. Fu, 2001: Contributions of photon tunneling to extinction in laboratory grown hexagonal columns. *J. Quant. Spectroscopy and Radiative Trans.*, **70**, 761-776.

Mitchell, D.L., 2002: Effective diameter in radiation transfer: Definition, applications and limitations. *J. Atmos. Sci.*, **59**, 2330-2346.

Mitchell, D.L., and A.J. Baran, 2002: Testing of the modified anomalous diffraction approximation with T-matrix calculations for hexagonal columns. Preprints, 11th Conference on Atmospheric Radiation, AMS, 3-7 June 2002, Ogden, Utah, J139-J144.

Platt, C.M.R., J.D. Spinhirne, and W.D. Hart, 1989: Optical and microphysical properties of a cold ice cloud: Evidence for regions of small ice particles. *J. Geophys. Res.*, **94**, 11151-11164.

Platt, C.M.R., S.A. Young, P.J. Manson, G.R. Patterson, S.C. Marsden, R.T. Austin and J.H. Churnside, 1998: The optical properties of equatorial cirrus from observations in the ARM Pilot Radiation Observation Experiment. *J. Atmos. Sci.*, **55**, 1977-1996.

Platt, C.M.R., R.T. Austin, S.A. Young, G.R. Patterson, D.L. Mitchell and S.D. Miller, 2002: LIRAD observations of tropical cirrus clouds in MCTEX. Part I: Optical properties and detection of small particles in cold cirrus. Accepted for publ. in J. Atmos. Sci.

Smith, W.L., H.E. Revercomb, R.O. Knuteson, F.A. Best, R. Dedecker, H.B. Howell, and H.M. Woolf, 1995: Cirrus cloud properties derived from high spectral resolution infrared spectrometry during FIRE II. Part I: The high resolution interferometer sounder (HIS) systems. *J. Atmos. Sci.*, **52**, 4238-4245.